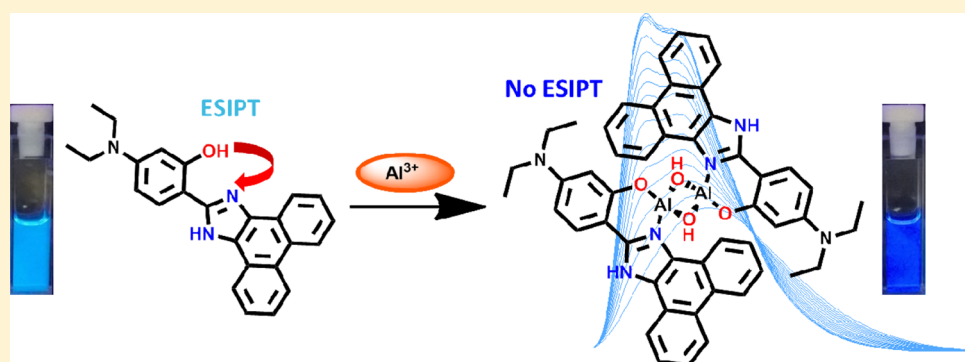


A Highly Sensitive ESIPT-Based Ratiometric Fluorescence Sensor for Selective Detection of Al³⁺

Sanghamitra Sinha, Bijit Chowdhury, and Pradyut Ghosh^{*,†}

[†]Department of Inorganic Chemistry, Indian Association for the Cultivation of Science, 2A & 2B Raja S. C. Mullick Road, Kolkata 700 032, India

S Supporting Information



ABSTRACT: An excited-state intramolecular proton transfer (ESIPT)-based highly sensitive ratiometric fluorescence sensor, 1H was developed for selective detection of aluminum (Al³⁺) in acetonitrile as well as in 90% aqueous system. Single-crystal X-ray diffraction analysis reveals almost planar and conjugated structure of 1H. Photophysical properties of the sensor as well as its selectivity toward Al³⁺ are explored using UV–visible, steady-state, and time-resolved fluorescence spectroscopic studies. The bright cyan ($\lambda_{em} = 445$ nm) fluorescence of 1H in acetonitrile turns into deep blue ($\lambda_{em} = 412$ nm) with ~ 2.3 -fold enhancement in emission intensity, in the presence of parts per billion level Al³⁺ (detection limit = 0.5 nM). Interestingly, the probe 1H exhibits increased selectivity toward Al³⁺ in H₂O/acetonitrile (9:1 v/v) solvent system with a change in fluorescence color from pale green to deep blue associated with ca. sixfold enhancement in emission intensity. Density functional theoretical (DFT) calculations provide the ground- and excited-state energy optimized structures and properties of the proposed aluminum complex [Al(1)(OH)₂]²⁺, which is in harmony with the solution-state experimental findings and also supports the occurrence of ESIPT process in 1H. The ESIPT mechanism was also ascertained by comparing the basic photophysical properties of 1H with a similar O-methylated analogue, 1'Me.

INTRODUCTION

During the past few years, a huge amount of research interest has been devoted to the area of sensing of trace metal ions because of their numerous effects on the biosphere.^{1a–k,2a–h,3a–l} However, the number of reports on effective aluminum sensing is still limited.^{2a–i} Aluminum is the most abundant ($\sim 8\%$ of the earth surface) metal in the planet and is mostly present in its ionic form Al³⁺, in atmosphere.^{4a–c,5a–m} Increased concentration of aluminum is poisonous for aquatic species like fish, algae, bacteria, plants, etc. and also hazardous to human health.^{4a–d} According to World Health Organization, the bearable aluminum intake for a human body is estimated to be 7 mg week^{−1} kg^{−1} body weight.^{4a–d,5a–m} In this context, development of fluorescent probes for Al³⁺ is becoming increasingly more common to address the sensibility issue.^{4a–d,5a–o} But achieving this goal has been found to be comparatively more difficult than that for the other metal ions because of the poor coordination ability, strong hydration aptitude, and the lack of spectroscopic characteristics of Al³⁺. Being a hard acid, Al³⁺ prefers to bind with hard base.^{4c,d}

Exploiting this idea a number of oxygen- and nitrogen-rich chelating ligands like Schiff bases,^{6a–g} imidazoline,²ⁱ 8-hydroxyquinoline^{4d}-based fluorescence turn-on Al³⁺ sensors have been reported, where the mechanisms utilized are mostly based on chelation-enhanced fluorescence,⁷ photoinduced electron transfer (PET),^{2i,4b,8a,b} metal–ligand charge transfer,^{5e} etc. Most of these show enhanced emission intensity with little or no spectral shift,^{4a–d} and Schiff-base derivatives are generally prone to hydrolysis in aqueous system.⁹ In recent years, excited-state intramolecular proton transfer (ESIPT) process and ratiometric fluorescence sensing have come into the limelight due to their theoretical and practical importance.^{3a–k,10} ESIPT is a fast (picosecond) intramolecular proton-transfer process, occurs in excited state of suitable molecules containing –OH/–NH/–SH, C=N/C=O, etc. functionalities, which results large Stokes shift.¹⁰ A very few fluorescence turn-on ESIPT-based sensors for Al³⁺ have been reported; however, those are based on Schiff-base

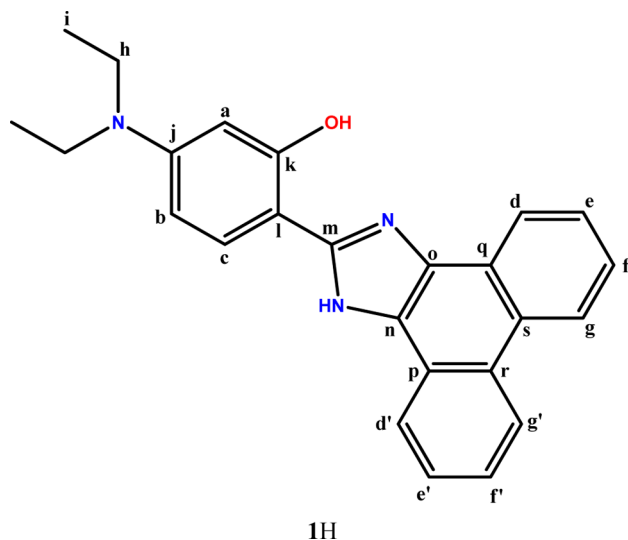
Received: May 12, 2016

generated skeleton.^{5f,11a,b} Thus, development of aqueous stable ESIPT-based ratiometric sensor for Al^{3+} remains a challenging task. In this work, we developed a simple ratiometric ESIPT-based non-Schiff-base fluorescent sensor 1H, which can selectively detect Al^{3+} in parts per billion level both in organic and in 90% aqueous system even in the presence of excess amount of other metal ions.

RESULTS AND DISCUSSION

Designing Aspect of 1H. Among varieties of ESIPT-based ligands, 2-(2-hydroxyphenyl)benzoxazole (HBO), 2-(2-hydroxyphenyl)benzothiazole (HBT), and 2-(2-hydroxyphenyl)benzimidazole (HBI) derivatives have turned out to be the most promising sensors due to their preferential photophysical properties like large Stokes shift and distinctly different coloration upon guest binding with very high selectivity and sensitivity in the recent years.^{3e} Besides these, they can also provide hard basic chelating sites containing oxygen and nitrogen, which would be favorable for aluminum binding. However, HBI derivatives possess higher quantum yields than those of HBO and HBT.^{3e} Keeping these things in mind an HBI-based ligand (1H) was designed, where a diethylamino phenolic unit is coupled with 9,10-phenanthrene imidazole moiety resulting in a highly conjugated intramolecularly proton transferable structure (Chart 1). The phenanthrene unit was

Chart 1. Chemical Structure of the Ligand 1H



attached to extend the delocalization as well as to improve the quantum efficiency by reducing nonradiative deactivation via rigidification of the structure. It is expected that the ESIPT unit itself, due to its hard basic nature, would act as the coordinating

site toward aluminum. Further to ascertain the role of $-\text{OH}$ group in Al^{3+} binding via tuning the ESIPT mechanism, a similar O -methylated system (1'Me) was developed.

Synthesis and Characterization. Sensor 1H is synthesized by refluxing 9,10-phenanthrenequinone, 4-(diethylamino)-2-hydroxybenzaldehyde, and ammonium acetate in glacial acetic acid for 4 h. It is fully characterized by ^1H , $^1\text{H}-^1\text{H}$ COSY, ^{13}C and ^1H DEPT-135-HSQC NMR, (Scheme 1 and Figures S1–S4, Supporting Information), electrospray ionization mass spectrometry (ESI-MS; Figure S5, Supporting Information), and elemental analysis techniques. Finally, the solid-state structure of 1H is confirmed by single-crystal X-ray diffraction analysis. In the NMR spectrum of 1H, all the protons and carbons resonate at their expected frequency ranges, while the protons of $-\text{OH}$ and $-\text{NH}$ groups resonate downfield near 13 ppm. This could be due to the intramolecular hydrogen bond formation between phenolic $-\text{OH}$ proton with nitrogen of imidazole $\text{C}=\text{N}$ and intermolecular hydrogen bond between $-\text{NH}$ proton and the oxygen in deuterated dimethyl sulfoxide ($\text{DMSO}-d_6$). In ESI-MS of 1H a single peak for molecular ion ($[\text{C}_{25}\text{H}_{23}\text{N}_3\text{O}][\text{H}^+]$) is observed at 382.14 (calculated 382.18). Synthesis and characterization of 1'Me are given in Scheme S1 and Figures S6 and S7, Supporting Information.

Single Crystal X-ray Diffraction Analysis. Diffractable quality single crystals of 1H are obtained by slow evaporation from its ethyl acetate–petroleum ether (1:5) solution at room temperature. 1H crystallizes in orthorhombic crystal system with $Pbca$ space group. Asymmetric unit of the crystal contains one ligand molecule and one ethyl acetate (Figure 1 and Figure S8,

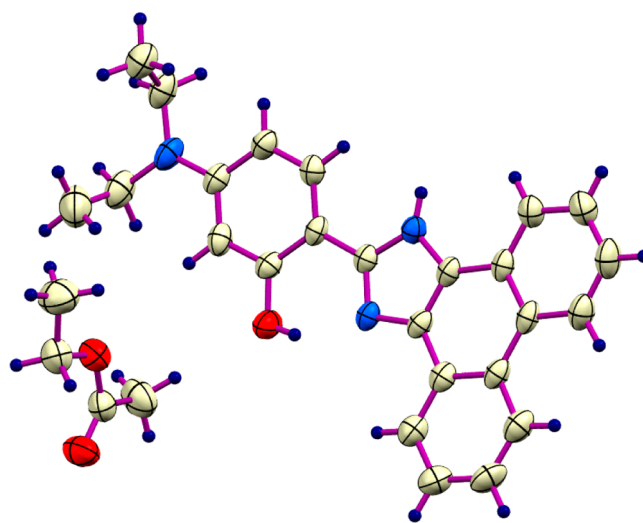
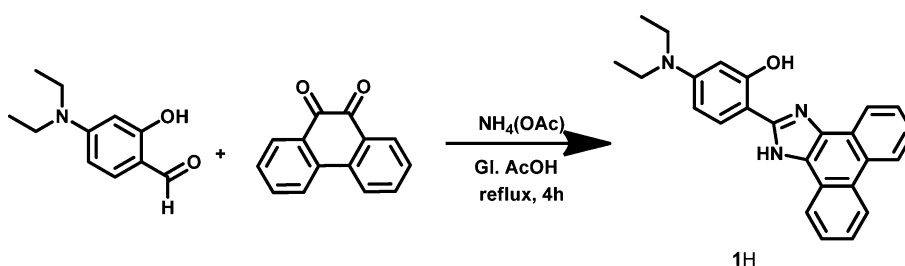


Figure 1. Single-crystal X-ray structure of the ligand 1H (thermal ellipsoids are drawn at 50% probability level). Color code: O, red; N, blue; C, gray; H, dark blue.

Scheme 1. Synthetic Scheme of the Ligand 1H



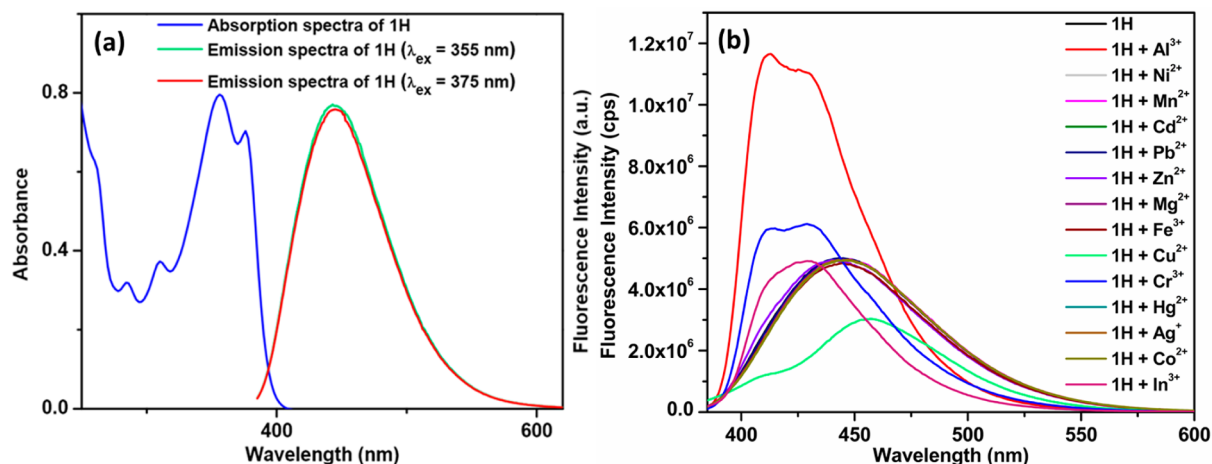


Figure 2. (a) UV–vis and fluorescence spectra of 1H, measured in acetonitrile at room temperature (concentration: 20 and 2.5 μM , respectively). (b) Fluorescence (2.5 μM) spectral changes of 1H in the presence of various metal ions (10 equiv) as their perchlorate salts, in acetonitrile at room temperature.

Supporting Information). Detailed crystallographic parameters are listed in Table S1, Supporting Information. Structural analysis reveals that the molecule is almost planar and highly conjugated.

Al³⁺ Sensing Studies in Acetonitrile. Photophysical properties of the ligand are thoroughly studied using absorbance (UV–visible), photoluminescence (PL), and time-resolved spectroscopic methods. UV–vis spectrum of 1H has a prominent signature of the chromophoric phenanthrene unit. It shows bands at ~ 243 ($\epsilon = 41\,350\text{ M}^{-1}\text{ cm}^{-1}$), ~ 260 ($\epsilon = 30\,235\text{ M}^{-1}\text{ cm}^{-1}$), ~ 284 ($\epsilon = 15\,572\text{ M}^{-1}\text{ cm}^{-1}$), ~ 310 ($\epsilon = 18\,150\text{ M}^{-1}\text{ cm}^{-1}$), ~ 355 ($\epsilon = 38\,600\text{ M}^{-1}\text{ cm}^{-1}$), and $\sim 375\text{ nm}$ ($\epsilon = 34\,100\text{ M}^{-1}\text{ cm}^{-1}$) in acetonitrile at 25 $^{\circ}\text{C}$ (Figure 2a), among which the first three bands at 243, 260, and 284 nm can be considered as intraligand (IL) $\pi\text{--}\pi^*$ transitions. The bands at 310, 355, and 375 nm may be due to the electronic transitions from nonbonding orbitals on the heteroatoms to ligand π^* orbitals, that is, $n\text{--}\pi^*$ transition.^{12a} Excitation at either 355 or 375 nm wavelengths results in a large Stokes shift giving the same emission profile consisting of an intense emission band at 445 nm (Figure 2a). It indicates that whatever the excitation energy is, emission is occurring from the same excited singlet state, making the molecule highly fluorescent with bright cyan color under UV irradiation. Such a large Stokes shift can be explained by comparatively low energy gap between keto excited state and the keto ground state (than that in the enol form), which like the other ESIPT systems should be responsible for the emission spectra of the molecule (Chart S1, Supporting Information).^{10,11a,b} This may be visualized from the computational energy level diagram that will be described later. The ESIPT process in 1H is further confirmed by UV–vis and PL studies of the control compound 1'Me, where ESIPT cannot occur (Figure S9, Supporting Information). It shows only 45 nm ($\sim 3169\text{ cm}^{-1}$) Stokes shift, which can be originated from nonradiative vibrational decays, the reason for Stokes shifts in normal fluorescent molecules.

Metal binding properties of 1H are investigated to check its selectivity toward metal ions. Addition of various metal ions (10 equiv) as their corresponding perchlorate salts to 20 μM solution of 1H in acetonitrile results red shift of the absorption bands from 355 and 375 nm to 375 and 390 nm, respectively, with an increase in absorbance in case of Al³⁺ (Figure S10, Supporting Information). A clear isosbestic point is observed at 363 nm.

Absorption spectrum does not change significantly in the presence of other metal ions except in case of Cr³⁺, where a similar spectral shift is observed without any prominent change in absorbance.

A large change in the emission spectra of 1H (2.5 μM in acetonitrile) is observed upon addition of a very small amount of Al³⁺ (Figure 2b). The peak at 445 nm diminishes, while two new peaks appear at 412 and 430 nm with ~ 2.3 -fold higher intensity. Cr³⁺ and In³⁺ show same shift at higher concentration, where the increase in intensity is much less (Figure 2b and Figure S11, Supporting Information). However, Cu²⁺, because of its paramagnetic quenching property, reduces the fluorescence intensity of 1H, while the other metal ions remain silent to this system. The change in absorption and emission spectra of 1H in the presence of Al³⁺ can easily be correlated with the theoretically computed energy-level diagram of the frontier molecular orbitals of the free receptor and its Al³⁺ complex, which will be discussed later in the theoretical part. On the one hand, the energy difference between highest occupied molecular orbital (HOMO) and lowest unoccupied molecular orbital (LUMO) in the Al³⁺ complex is less compared to that of 1H(enol), which is responsible for the ligand absorption profile, and thus it shows a bathochromic shift in the UV–visible spectrum upon metal coordination. On the other hand, the same difference is greater than that of the keto form, which may be responsible for the ligand emission profile, thus leading to hypsochromic shift of fluorescence peaks. However, the fluorescence spectrum of 1'Me shows 10 nm bathochromic shift that can be rationalized by the lowering of the HOMO–LUMO energy gap upon Al³⁺ coordination (Figure S9, Supporting Information).

Considering quinine sulfate as standard,^{11c} the quantum yield (ϕ_f) value of 1H comes out to be 0.424 (Figure S12, Supporting Information). This high ϕ_f value in solution state may be the outcome of the intramolecular hydrogen bonding between phenolic –OH and the imidazole N, which makes the molecule rigid, by restricting rotation about the single bond connecting diethylaminophenolic and the phenanthrene–imidazole unit, and lowers the nonradiative decays via rotational and vibrational relaxation pathways. Complexation with Al³⁺ further increases the quantum yield value to 0.5474, which may be attributed to more rigidification by metal coordination via deprotonation and

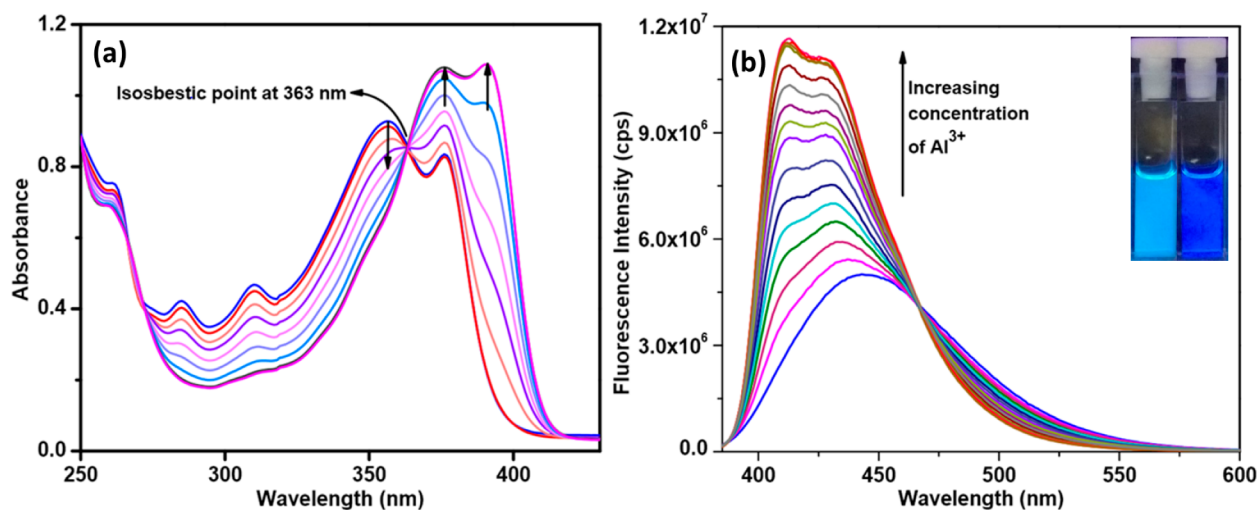


Figure 3. (a) UV-vis ($20\ \mu\text{M}$) and (b) fluorescence ($2.5\ \mu\text{M}$) titration profiles of 1H with Al^{3+} in acetonitrile at room temperature. (inset) Fluorescence colors of 1H (left) and its Al^{3+} complex (right) in acetonitrile.

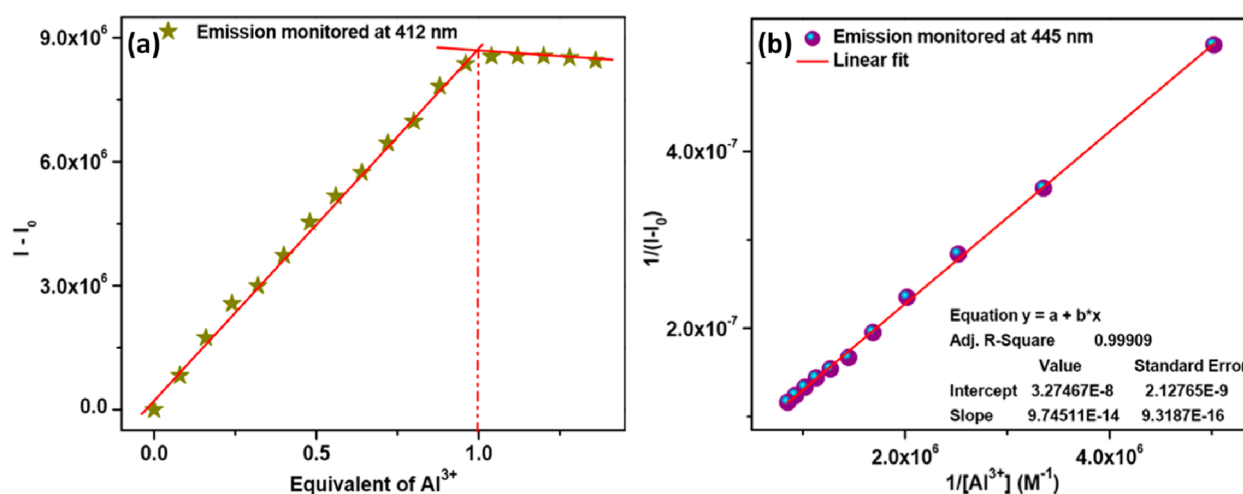


Figure 4. (a) An equivalent plot from PL titration data of 1H ($2.5\ \mu\text{M}$) with Al^{3+} and (b) Benesi–Hildebrand plot for calculation of association constant from PL titration of ligand 1H with Al^{3+} in acetonitrile at room temperature.

hard–hard interaction than the rigidification by comparatively weaker H-bond formation.

For better understanding the Al^{3+} binding properties of 1H, absorption and fluorescence titration experiments are performed. Upon incremental addition of Al^{3+} into acetonitrile solution of 1H ($20\ \mu\text{M}$) a red shift in the absorption bands is observed. The absorbance at $355\ \text{nm}$ is gradually decreased with concomitant increase in the absorbance at $375\ \text{nm}$ and simultaneous development of a new peak at $390\ \text{nm}$ (Figure 3a). After addition of 1 equiv of Al^{3+} , saturation point is reached, and no more change is observed in the absorption spectrum (Figure S13a, Supporting Information). A single isosbestic point at $363\ \text{nm}$ indicates the presence of two species: the free ligand and the ligand– Al^{3+} complex. Job's plot analysis shows inflection point at 0.5, suggesting 1:1 host–guest stoichiometric binding event (Figure S13b, Supporting Information). PL titration experiment is performed by gradually adding Al^{3+} into the acetonitrile solution of 1H ($2.5\ \mu\text{M}$). With increasing concentration of Al^{3+} , the strong emission band at $445\ \text{nm}$ is gradually blue-shifted, and two new emission maxima at $412\ \text{nm}$ and $430\ \text{nm}$ are observed (Figure 3b). Intensities of these peaks increase up to addition of 1 equiv of Al^{3+} (Figure 4a), after which saturation point is achieved,

and no further increase in the fluorescence intensity is observed. Enhancement of intensity is ~ 2.3 -fold as compared to the free ligand. The Job's plot analysis reveals 1:1 host–guest stoichiometry between 1H and Al^{3+} (Figure S14, Supporting Information). Binding constant is calculated as $3.36 \times 10^5\ \text{M}^{-1}$, from Benesi–Hildebrand plot analysis (Figure 4b).

To check the selectivity of 1H toward Al^{3+} , the change in fluorescence intensity of the ligand upon addition of 1 equiv of Al^{3+} is monitored in the presence of excess amount of other competitive metal ions (e.g., Cr^{3+} , In^{3+} , Cu^{2+} , Mn^{2+} , Mg^{2+} , Ag^{2+} , Hg^{2+} , Zn^{2+} , Pb^{2+} , Fe^{3+} , Ni^{2+} , and Co^{2+} ; 10 equiv each). As shown in Figure S15a, Supporting Information, the selectivity along with the emission enhancement remains almost unperturbed in the presence of all metal ions. A plot of fluorescence intensity change ($I - I_0$) versus concentration of Al^{3+} yields the detection limit as low as $0.5\ \text{nM}$, which is much lower than the maximum tolerable limit of Al^{3+} (Figure S15b, Supporting Information). Such a low detection limit as well as the selective emission enhancement and large blue shift with Al^{3+} reach to a conclusion that 1H is an effective sensor for selective detection of Al^{3+} even in the presence of a large excess of other competitive metal ions in acetonitrile.

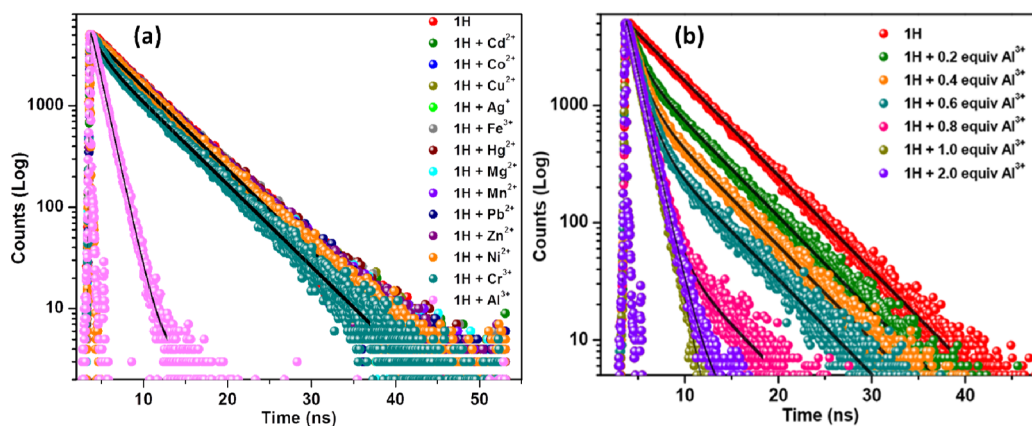


Figure 5. Time-resolved luminescence decays of 1H ($2.5 \mu\text{M}$; $\lambda_{\text{em}} = 445 \text{ nm}$) (a) in the presence of various metal ions as their perchlorate salts and (b) upon addition of increasing amount of Al^{3+} in acetonitrile at room temperature.

Time-Resolved Spectroscopic Study. The conclusion made by steady-state spectroscopic measurements is again supported by fluorescence lifetime study. Lifetimes (τ) of free ligand (1H) and the ligand in the presence of various metal ions are determined using time-correlated single-photon count (TCSPC) experiment (Table S2, Supporting Information). Lifetime of 1H (5.37 ns) is decreased in the presence of Al^{3+} (1.14 ns), while no remarkable change is observed in the presence of other metal ions. Decay pattern of 1H also remains unchanged in the presence of all metal ions except Al^{3+} (Figure 5a). These observations indicate that the nature of the free ligand (1H) is retained in cases of all other metal ions. Moderate lifetime value as well as high quantum yield of 1H suggests that the rate of nonradiative decay (κ_{nr}) is not large in 1H. This can also be explained by the formation of intramolecular hydrogen bond between phenolic $-\text{OH}$ and imidazole N, which rigidifies the system and hence suppresses nonradiative decay pathways.

And this rigidification is strengthened by Al^{3+} coordination. So, κ_{nr} does not differ largely between 1H and its Al^{3+} adduct, and unlike most of the cases, here it is not the governing factor for lifetime determination. The radiative decay rate (Γ), which is an intrinsic property of a fluorophore and depends on its absorption and emission spectra and refractive index of the medium, plays a major role in this case.^{12b} Coordination with Al^{3+} ion shifts the excitation and emission maxima as well as increases the absorbance and fluorescence intensity, resulting in an increase in radiative decay rate of Al^{3+} complex as compared to that of 1H, which is reflected in their corresponding lifetime values. No change in decay pattern of 1H with other metal ions indicates that no adduct is formed with these metal ions, because of which ligand is the only contributor to the overall lifetime. Titration with Al^{3+} shows gradual decrease in lifetime with change in the decay pattern from single exponential to biexponential and finally again to single exponential at 1 equiv of Al^{3+} , which remains unchanged upon further addition of Al^{3+} (Figure 5b; Table S3 and Figure S16a, Supporting Information). This observation suggests that initially free ligand is the only species present in solution and is the solitary contributor to lifetime value. Incremental addition of Al^{3+} increases the concentration of the Al^{3+} adduct, which starts to contribute in overall lifetime, resulting in biexponential decay with shorter lifetime. After addition of 1 equiv of Al^{3+} , all the ligand molecules undergo adduct formation with Al^{3+} resulting in Al^{3+} complex, having shorter lifetime, as the solitary contributor to the new single-exponential decay. The similar decay pattern as well as the

lifetime values of 1H (5.35 ns) and 1H in the presence of Al^{3+} (1.27 ns) at longer wavelength (525 nm) again support the ESIPT mechanism (Figure S16b, Supporting Information).

Al^{3+} Sensing by 1H in Aqueous Medium. In aqueous environment metal ions generally remain surrounded by solvent media, which makes it difficult to sense metal ions in water. To check whether the selective sensing property of 1H toward Al^{3+} is retained in aqueous environment, UV–visible and PL studies are performed with various metal ions (e.g., Cr^{3+} , In^{3+} , Cu^{2+} , Mn^{2+} , Mg^{2+} , Ag^{2+} , Hg^{2+} , Zn^{2+} , Pb^{2+} , Fe^{3+} , Ni^{2+} , Co^{2+} , and Al^{3+}) in $\text{H}_2\text{O}/\text{acetonitrile}$ (9:1 v/v) solvent system, where the metal ions are taken in 100% water. Absorption spectrum of 1H shows two strong bands at 246 nm ($\epsilon = 26\,283 \text{ M}^{-1} \text{ cm}^{-1}$) and 366 nm ($\epsilon = 22\,461 \text{ M}^{-1} \text{ cm}^{-1}$), whereas excitation at 366 nm results emission at $\sim 463 \text{ nm}$. Fluorescence intensity of 1H is less in case of $\text{H}_2\text{O}/\text{acetonitrile}$ (9:1 v/v) solvent as compared to that in acetonitrile (Figure S17, Supporting Information). Ligand 1H shows greater selectivity toward Al^{3+} in $\text{H}_2\text{O}/\text{acetonitrile}$ (9:1 v/v) solvent with \sim sixfold enhancement in fluorescence intensity, associated with a change in fluorescence color from pale green to blue (Figure 6a). However, a large excess of Cr^{3+} and In^{3+} causes same color change as Al^{3+} with very small increase in intensity. The improvement in selectivity toward Al^{3+} in aqueous solvent can be explained by the hard–hard interaction between N- and O-containing chelating site of 1H and strong Lewis acidic Al^{3+} that allows 1H to overcome the high solvation energy barrier in case of Al^{3+} , which is not possible for rest of the metal ions.

Absorbance and fluorescence titration experiments are performed by gradually adding Al^{3+} (dissolved in water) into a $\text{H}_2\text{O}/\text{acetonitrile}$ (9:1 v/v) solution of 1H, to understand the binding properties of 1H with Al^{3+} . Incremental addition of Al^{3+} results in a steady decrease in the absorbance at 366 nm with simultaneous formation of a new band at 430 nm associated with an isosbestic point at 405 nm (Figures S18 and S19, Supporting Information). In fluorescence titration, upon addition of Al^{3+} the emission band at 463 nm shifts toward higher energy region resulting in a new emission band containing two peaks at 412 and 430 nm (Figure 6b). Intensities of the peaks are increased gradually to \sim sixfold as that of the free ligand. Saturation point is reached at 1 equiv of Al^{3+} , which, along with the corresponding Jobs plot analysis, proves 1:1 stoichiometric binding between 1H and Al^{3+} (Figure 6c and Figure S20, Supporting Information). Association constant between 1H and Al^{3+} is determined from Benesi–Hildebrand plot as $8 \times 10^4 \text{ M}^{-1}$, which is less as compared to that in acetonitrile (Figure S21a, Supporting

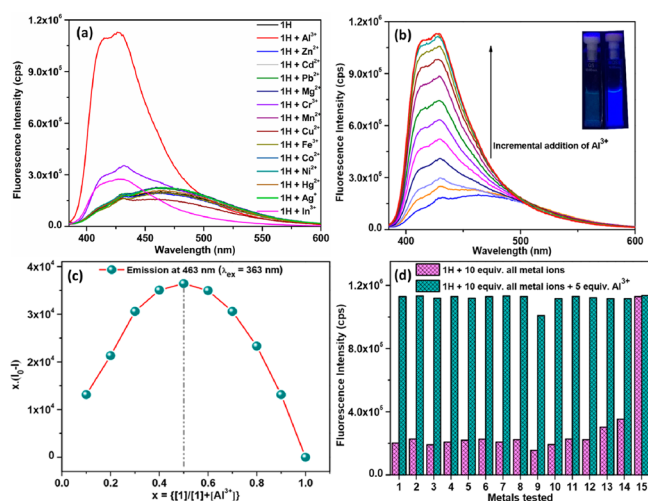


Figure 6. (a) Fluorescence ($2.5 \mu\text{M}$) spectral changes of 1H in the presence of various metal ions (10 equiv). (b) Fluorescence titration profile of 1H ($2.5 \mu\text{M}$) with Al^{3+} . (inset) Fluorescence colors of 1H (left) and its Al^{3+} complex (right) in $\text{H}_2\text{O}/\text{acetonitrile}$ (9:1 v/v). (c) Corresponding Job's plot experiment of 1H ($7.5 \mu\text{M}$) with Al^{3+} ($7.5 \mu\text{M}$). (d) Selectivity graph of 1H with Al^{3+} in the presence of other metal ions in $\text{H}_2\text{O}/\text{acetonitrile}$ (9:1 v/v) solvent at room temperature ($\lambda_{\text{em}} = 412 \text{ nm}$ for Al^{3+} , Cr^{3+} , and In^{3+} and 463 nm for other metal ions). (pink) Fluorescence intensities of 1H in the presence of all metal ions (10 equiv). (green) Fluorescence intensities in the presence of all metal ions and Al^{3+} . Codes used: (1) only 1H, (2) Ag^+ , (3) Zn^{2+} , (4) Cd^{2+} , (5) Pb^{2+} , (6) Mn^{2+} , (7) Hg^{2+} , (8) Mg^{2+} , (9) Cu^+ , (10) Fe^{3+} , (11) Co^{2+} , (12) Ni^{2+} , (13) In^{3+} , (14) Cr^{3+} , (15) Al^{3+} .

Information). Detection limit (12 nM) of 1H for Al^{3+} is higher in $\text{H}_2\text{O}/\text{acetonitrile}$ (9:1 v/v) binary solvent than in acetonitrile (Figure S21b, Supporting Information).

To check the selectivity of 1H toward Al^{3+} in the presence of other metal ions in $\text{H}_2\text{O}/\text{acetonitrile}$ (9:1 v/v), change in fluorescence intensity of 1H upon addition of 1 equiv of Al^{3+} (in 100% water) is monitored in the presence of excess amount of other competitive metal ions (10 equiv each). The result shows same fluorescence enhancement with Al^{3+} as in absence of competitive metal ions (Figure 6d). The time-resolved fluorescence titration data in $\text{H}_2\text{O}/\text{acetonitrile}$ (9:1 v/v) solvent (Figure S22, Supporting Information) shows gradual decrease in lifetime of 1H upon incremental addition of Al^{3+} , which stops beyond 1 equiv of Al^{3+} . The small lifetime of 1H (36 ps) suggests that ESIPT process becomes weaker in aqueous system. Further it is observed that the pH of the solution before and after the addition of Al^{3+} remains the same, which in turn justifies the fact that the observed change in emission profiles is solely due to the binding of Al^{3+} and not to the effect of pH. On the one hand, the sensing efficiency of 1H is decreased in acidic pH, which may be due to the protonation of imidazole nitrogen atoms as well as prohibition of the deprotonation of phenolic $-\text{OH}$ group, which is necessary for Al^{3+} coordination. On the other hand, at alkaline pH, OH^- ions compete for Al^{3+} with the ligand, which reduces the sensitivity of 1H toward Al^{3+} .^{11a} Thus, the overall result suggests that 1H can be used as an even better fluorescent sensor for Al^{3+} in $\text{H}_2\text{O}/\text{acetonitrile}$ (9:1 v/v) system than in pure acetonitrile.

Mechanistic Investigation using ^1H Nuclear Magnetic Resonance Spectroscopy and Electrospray Ionization Mass Spectrometry. To understand the mechanism of Al^{3+} binding by 1H, ^1H NMR spectroscopic titration experiment is

performed in $\text{DMSO}-d_6$ solvent. Incremental addition of Al^{3+} into a $\text{DMSO}-d_6$ solution of 1H broadens the peaks of $-\text{OH}$ and $-\text{NH}$ protons at 13.26 and 12.99 ppm, respectively. Intensity of the $-\text{OH}$ peak decreases slowly, and it disappears at 1 equiv of Al^{3+} concentration (Figure 7). All the spectral changes continue

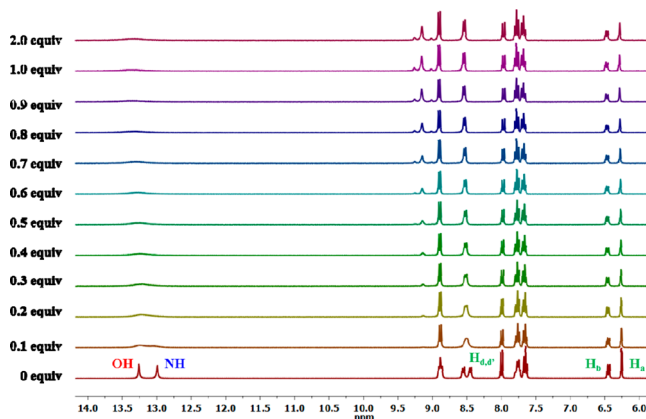
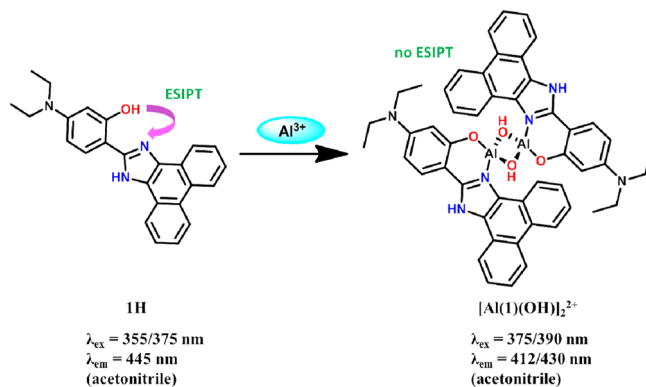


Figure 7. Changes in ^1H NMR spectra of 1H (7.9 mM) upon addition of increasing amounts of Al^{3+} in $\text{DMSO}-d_6$ at room temperature.

to that point only, after which saturation is reached. The results indicate breaking of the intramolecular H bond between phenolic $-\text{OH}$ and imidazole nitrogen ($\text{C}=\text{N}$), followed by deprotonation of the phenolic proton in the presence of Al^{3+} .

The two isolated doublets at 8.545 and 8.445 ppm in free ligand NMR spectrum, corresponding to H_d and H_e protons, merge into a single doublet in the presence of Al^{3+} . This result may be explained by the deprotonation of phenolic proton, which along with the metal coordination indirectly equalizes the electronic environment around these two apparently electronically nonequivalent protons. ^1H NMR titration experiment is also performed in 1:1 $\text{D}_2\text{O}/\text{CD}_3\text{CN}$ solvent, which shows downfield shifts of the H_a , H_b , and H_c peaks (Figure S23, Supporting Information). Effect of Al^{3+} on $-\text{OH}$ and $-\text{NH}$ peaks could not be monitored, as these two peaks get broadened in polar protic solvent. The overall outcome suggests that deprotonation of the phenolic $-\text{OH}$ group as well as the hard-hard interaction between Al^{3+} and the O^- (of phenolate anion) and N (of imidazole $\text{C}=\text{N}$) atom of the ligand are the key factors in binding toward Al^{3+} (Scheme 2 and Figure S24, Supporting Information).

Scheme 2. Proposed Binding Mechanism of 1H with Al^{3+}



The ESI-MS of the isolated Al^{3+} complex of 1H shows peaks at 424.34 and 887.76 m/z , which could be assigned for $[\text{Al}(\text{I})(\text{OH})_2]^{2+}$ and $[\text{Al}(\text{I})(\text{O})_2]\text{K}^+$, respectively. Distribution pattern of both 1+ and 2+ charged species match well with their corresponding theoretically calculated patterns (Figures S25 and S26, Supporting Information). This approximated structure agrees with the experimental findings as well as the previous reports³¹ and the three-centered two-electron bond formation property of aluminum.^{2h,51} Several trials to get crystals of the Al^{3+} complex failed. So DFT calculations are made to ascertain the proposed structure of the Al^{3+} complex as well as the ESIPT mechanism.

Theoretical Calculations and Molecular Orbital Analysis of 1H and Its Al^{3+} Complex. To get insight into the sensing mechanism and the structure–property relationship of the $[\text{Al}(\text{I})(\text{OH})_2]^{2+}$ dimer, ground (S_0) and excited states (S_1) are performed with hybrid B3LYP functional^{12c} as incorporated in Gaussian 09 package,^{12d} mixing the exact Hartree–Fock-type exchange with Becke’s exchange functional^{12e} and that proposed by Lee–Yang–Parr for the correlation contribution.^{12f} The 6-311G(d)^{12g} basis set is used for all the atoms with conductor-like polarizable continuum model (CPCM)^{12h} for acetonitrile solvent (Figure 8 and Figures

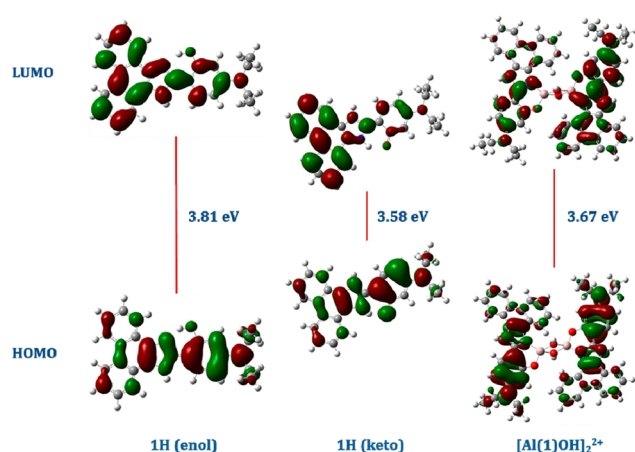


Figure 8. Frontier molecular orbitals of 1H and $[\text{Al}(\text{I})(\text{OH})_2]^{2+}$ with their corresponding energy gap as calculated from DFT B3LYP/6-311G(d) computational level using CPCM model for acetonitrile [isovalue = 0.02].

S27 and S28, Supporting Information). Theoretical outcome shows that in ground state, 1H is present in its enol form, as it possesses lower energy than the corresponding keto ground state. But after excitation, tautomerization becomes favored toward the excited keto form. This is because of the lower energy of keto S_1 state as compared to that of enol S_1 . Thus, the absorption spectrum of ligand 1H nicely matches with the theoretically calculated UV–visible spectrum of the enol form (Figure S29, Supporting Information). Details about the electronic transitions are given in Table S4, Supporting Information. The ground-state optimized structure of 1H is consistent with its single-crystal structure. As depicted in Figure 8 and Figure S28, Supporting Information, both the HOMO and LUMO of 1H (in enol as well as keto form) are almost evenly distributed on overall ligand molecule, which reduces the chance of PET process from diethylamino group of the molecule to the phenanthrene moiety, which could result in fluorescence quenching in this type of molecule. This, along with the

restricted rotation around C–C single bond between phenyl and imidazole ring, is responsible for high quantum efficiency of the ligand 1H. The energy difference between HOMO and LUMO is in the order of 1H (enol) > $[\text{Al}(\text{I})(\text{OH})_2]^{2+}$ > 1H (keto). Ground-state optimized structure of $[\text{Al}(\text{I})(\text{OH})_2]^{2+}$ shows the presence of Al–O–Al three-centered two-electron bonds, where the Al–O bond lengths are ~ 1.83 and 1.84 Å (Figure S27 and Tables S5 and S6, Supporting Information). Phenolic O and imidazole N (C=N) act as the chelating site and form coordinate bonds with Al center with a bite angle of $\sim 102^\circ$. The Al–O–Al bond angle is observed as $\sim 101^\circ$, while $\angle \text{O–Al–O}$ is $\sim 80^\circ$. The bond angles around Al vary from $\sim 80^\circ$ to $\sim 127^\circ$, which suggests a distorted tetrahedral geometry around both the Al centers. This is in accord with the literature reports on 3c–2e bond formation by Al.^{2h,31,51} Frontier molecular orbitals in $[\text{Al}(\text{I})(\text{OH})_2]^{2+}$ are mainly laid on the ligand rather than on Al centers, where the HOMO is mostly contributed by phenolic imidazole part of the ligand, and LUMO spreads over total ligand moiety. In other words, it can be said that the absorption bands are only due to intraligand $n\text{--}\pi^*$ and $\pi\text{--}\pi^*$ electronic transitions not for charge transfer from metal to ligand or vice versa. Excitation energies of 1H and $[\text{Al}(\text{I})(\text{OH})_2]^{2+}$ are calculated, which show that the absorption bands at 355 and 375 nm for 1H correspond to HOMO-to-LUMO+1 and to HOMO-to-LUMO electronic transitions, respectively, while the 375 and 390 nm bands in $[\text{Al}(\text{I})(\text{OH})_2]^{2+}$ are mainly due to the electron transfer from HOMO–1 to LUMO and from HOMO to LUMO, respectively.

CONCLUSIONS

In conclusion, an ESIPT-based ratiometric fluorescent sensor, 1H, is developed, which can selectively detect Al^{3+} in parts per billion level, both in acetonitrile and in 90% H_2O –acetonitrile system. Ligand 1H exhibits two distinctly different colors in free form as well as in the presence of Al^{3+} . Higher selectivity of 1H toward Al^{3+} in 90% H_2O –acetonitrile solvent makes it suitable for real-life application. DFT calculations suggest the presence of 3c–2e bonds (Al–O–Al) with distorted tetrahedral geometry around aluminum in the resulting Al^{3+} complex. ESIPT-based sensing mechanism is also studied in molecular level using DFT. In summary, the work provides a new and effective fluorescence sensor for selective detection of Al^{3+} with an insight about its binding mechanism.

EXPERIMENTAL SECTION

Materials. The reaction and workup procedures were performed at ambient condition. Perchlorate salts of Al^{3+} , Cr^{3+} , Cu^{2+} , Mn^{2+} , Mg^{2+} , Ag^{2+} , Hg^{2+} , Zn^{2+} , Pb^{2+} , Fe^{3+} , Ni^{2+} , and Co^{2+} were purchased from Aldrich, and nitrate salts were purchased from Alfa Aesar; both of them were used as received. Glacial acetic acid was purchased from Spectrochem Pvt. Ltd., India. HPLC-grade solvents and doubly distilled water were used in spectral measurements. NMR solvent $\text{DMSO-}d_6$ was purchased from Aldrich.

Methods. Fourier transform infrared (FTIR) spectra were recorded on Shimadzu FTIR-8400S infrared spectrophotometer with KBr pellets. High-resolution mass spectrometry (HRMS) analysis was performed on QTOF–Micro YA 263 mass spectrometer in positive ESI mode. ^1H , ^{13}C , ^1H – ^1H COSY, and ^1H –DEPT-135-HSQC NMR experiments were performed on FT-NMR Bruker DPX 300/400/500 MHz NMR spectrometer, and chemical shifts for ^1H and ^{13}C NMR were reported in parts per million (ppm), calibrated to the residual solvent peak set. Absorption spectra were recorded in a PerkinElmer Lambda 900 UV/vis/NIR spectrometer (using quartz cuvette of 1 cm path length), and emission spectra were recorded in a FluoroMax-3 spectrophotometer, from Horiba Jobin Yvon. Elemental analysis was performed on PerkinElmer 2500 series II elemental analyzer, PerkinElmer, USA.

Picosecond diode laser (IBH Nanoled-07) was used to excite samples in an IBH Fluorocube apparatus for TCSPC measurements. The luminescence decays were recorded on a Hamamatsu MCP photomultiplier (R3809), and IBH DAS6 software was used to analyze the data. All geometry optimizations were performed with the Gaussian 09^{12d} program package using DFT. The B3LYP^{12c} functional and 6-311G(d) basis set^{12g} were used for all atoms. All geometries were fully optimized in the ground states (S_0). Time-dependent DFT calculations using CPCM^{12h} for acetonitrile solvent were performed to examine low-energy excitations at the ground-state geometry at the same level of calculation as employed for geometry optimizations. Gaussview5.0 was used for visualizations of the optimized structures and the MOs.

Caution! Metal perchlorate salts are extremely explosive in the presence of open flames and sparks or heat. Aluminum nitrate and perchlorate both are skin irritants. All due precautions should be taken while handling these.

Calculation of Association Constants. Association constant between 1H and Al^{3+} was calculated using UV and PL titration data. Association constants were calculated using Benesi–Hildebrand eq 1.

$$1/(I - I_0) = 1/(I - I_s) + 1/\{k(I - I_0)[Al^{3+}]\} \quad (1)$$

where I_0 is the PL intensity of free ligand (1H), and I is the PL intensity upon each addition of Al^{3+} . I_s is the PL intensity at saturation point. The errors were calculated within 10%.

Calculation of Detection Limit. Detection limit (DL) was calculated using the following eq 2:

$$DL = (3 \times SD)/\text{slope} \quad (2)$$

where SD corresponds to standard deviation of the blank sample, measured by 15 consecutive scans of the blank sample. Slope is obtained from the linear fit plot of PL intensity changes versus concentration of Al^{3+} added.

Calculation of Excited-State Lifetimes. Equation (3) was used to analyze the time-resolved emission decays:

$$P(t) = B + \sum_i a_i e^{-t/\tau_i} \quad (3)$$

where $P(t)$ is decay, i is the number of discrete emissive species, B is a baseline correction, a_i is the pre-exponential factor, and τ_i is the excited-state lifetime associated with the i th component, respectively. In case of multiexponential decays eq 4 was used to calculate average lifetime:

$$\langle \tau \rangle = \sum_i a_i \tau_i \quad (4)$$

where a_i is the contribution of the i th decay component, and $a_i = \alpha_i/\sum \alpha_i$.

X-ray Crystallographic Refinement Details. The crystallographic details of ligand 1H is given in Table S1, Supporting Information. A diffractable-size crystal was collected from the mother liquor, dipped in paratone oil, and then cemented on the tip of a glass fiber using epoxy resin. Intensity data of the crystal were collected using Mo $K\alpha$ ($\lambda = 0.7107 \text{ \AA}$) radiation on a Bruker SMART APEX diffractometer, equipped with a CCD area detector at 150 K. Data integration and reduction were processed by SAINT^{13a} software. Empirical absorption correction to the collected reflections was done by applying SADABS.^{13b} Structure was solved using SHELXTL¹⁴ and was refined on F^2 by the full-matrix least-squares technique using the SHELXL-97¹⁵ program package. PLATON-97¹⁶ and MERCURY 3.1¹⁷ were used to generate graphics. Additional crystallographic information is available in the Supporting Information.

Synthesis of 5-(Diethylamino)-2-(1H-phenanthro[9,10-d]-imidazole-2-yl)phenol (1H). A solution of 9,10-phenanthrenequinone (0.250 g, 1.2 mmol), 4-(diethylamino)-2-hydroxybenzaldehyde (0.232 g, 1.2 mmol), and ammonium acetate (1.5 g, 19.5 mmol) in glacial acetic acid (10 mL) was stirred at 90 °C for 4 h. The reaction mixture was poured into ice-cold water. Resulting precipitate was filtered, washed properly with water, and dried in air. The brownish-white residue was purified by medium-pressure column chromatography with silica gel of 60–120 mesh size using petroleum ether/ethyl acetate as eluent. Pure product was isolated at 20% ethyl acetate concentration as faded white powder (0.35 g, 77%). Elemental analysis: Calcd (%) for $C_{25}H_{23}N_3O$: C,

78.71; H, 6.08; N, 11.02; O, 4.19. Found: C, 78.25; H, 6.34; N, 11.56. FTIR in KBr disc (ν/cm^{-1}): 3315, 3057, 2974, 2924, 2897, 2868, 1699, 1637, 1568, 1527, 1489, 1456, 1416, 1375, 1354, 1302, 1277, 1225, 1198, 1148, 1080, 1043, 1014, 962, 854, 787, 756, 723, 656. ESI-MS [$C_{25}H_{23}N_3O$][H^+] calcd: m/z 382.18. Found: m/z 382.14. 1H NMR (300 MHz, DMSO- d_6 , Si(CH₃)₄): δ 13.26 (s, 1H, OH), 12.99 (s, 1H, NH), 8.88 (t, $J = 9$ Hz, 2H, H_{g,g'}), 8.54 (d, $J = 9$ Hz, 1H, H_d), 8.44 (d, $J = 9$ Hz, 1H, H_{d'}), 8.00 (d, $J = 9$ Hz, 1H, H_c), 7.76 (m, 2H, H_{e,e'}), 7.65 (t, $J = 9$ Hz, 2H, H_{f,f'}), 6.44 (d, $J = 9$ Hz, 1H, H_b), 6.25 (s, 1H, H_a), 3.41 (q, $J = 6$ Hz, 4H, H_h), 1.15 (m, 6H, H_i). ^{13}C NMR (100 MHz, DMSO- d_6 , Si(CH₃)₄): δ 159.2 (1C, C_k), 150.8 (1C, C_m), 149.9 (1C, C_j), 127.4–127.1 (4C, C_{p,q,r,s}), 126.8 (1C, C_c), 125.5–125.2 (6C, C_{e,e',f,f',o,n}), 124.1–123.8 (2C, C_{d,d'}), 121.8–121.6 (2C, C_{g,g'}), 103.5 (1C, C_l), 100.9 (1C, C_o), 98.0 (1C, C_a), 43.7 (2C, C_h), 12.59 (2C, C_i).

Synthesis of 2-(2-Methoxyphenyl)-1H-phenanthro[9,10-d]-imidazole (1'Me). A solution of 9,10-phenanthrenequinone (0.250 g, 1.2 mmol), 2-methoxybenzaldehyde (0.163 g, 1.2 mmol), and ammonium acetate (1.5 g, 19.5 mmol) in glacial acetic acid (8 mL) was stirred at 90 °C for 4 h. The reaction mixture was poured into ice-cold water. Resulting precipitate was filtered, washed properly with water, and dried. Pure product was obtained as faded white powder. (0.32 g, 83%). Elemental analysis: Calcd (%) for $C_{22}H_{16}N_2O$: C, 81.46; H, 4.97; N, 8.64; O, 4.93. Found: C, 81.22; H, 5.13; N, 8.31; O, 4.65. ESI-MS [$C_{22}H_{16}N_2O$][H^+] calcd: m/z 325.13. Found: m/z 325.03. 1H NMR (500 MHz, DMSO- d_6 , Si(CH₃)₄): 12.73 (s, 1H), 8.86 (d, $J = 8$ Hz, 2H), 8.64 (s, 2H), 8.23 (d, $J = 8$ Hz, 1H), 7.72 (t, $J = 8$ Hz, 2H), 7.63 (t, $J = 8$ Hz, 2H), 7.51 (t, $J = 8$ Hz, 1H), 7.28 (d, $J = 8$ Hz, 1H), 7.17 (t, $J = 8$ Hz, 1H), 4.04 (s, 3H).

ASSOCIATED CONTENT

Supporting Information

The Supporting Information is available free of charge on the ACS Publications website at DOI: 10.1021/acs.inorgchem.6b01170. CCDC No. 1475692 (L1) contains the supplementary crystallographic data for this paper. These data can be obtained free of charge from the Cambridge Crystallographic Data Centre via www.ccdc.cam.ac.uk/data_request/cif.

All NMR, ESI-MS, UV–vis, and PL titration data for 1H and Al^{3+} (PDF)

Crystallographic information file for 1H (CIF)

AUTHOR INFORMATION

Corresponding Author

*E-mail: icpg@iacs.res.in.

Notes

The authors declare no competing financial interest.

ACKNOWLEDGMENTS

P.G. gratefully acknowledges Science and Engineering Research Board, India, for financial support and Alexander von Humboldt Foundation for donating a fluorimeter. S.S. and B.C. would like to thank CSIR, India, for research fellowship. The authors acknowledge S. Mondal, IACS, for his help in theoretical calculations.

REFERENCES

- (1) Mikata, Y.; Yamanaka, A.; Yamashita, A.; Yano, S. *Inorg. Chem.* **2008**, *47*, 7295. (b) Mikata, Y.; Yamashita, A.; Kawamura, A.; Konno, H.; Miyamoto, Y.; Tamotsu, S. *Dalton Trans.* **2009**, 3800. (c) Mikata, Y.; Takeuchi, S.; Konno, H.; Iwatsuki, S.; Akaji, S.; Hamagami, I.; Aoyama, M.; Yasuda, K.; Tamotsu, S.; Burdette, S. C. *Dalton Trans.* **2014**, *43*, 10013. (d) Maity, S. B.; Bharadwaj, P. K. *Inorg. Chem.* **2013**, *52*, 1161. (e) Pal, S.; Chatterjee, N.; Bharadwaj, P. K. *RSC Adv.* **2014**, *4*, 26585. (f) Alfonso, M.; Tarraga, A.; Molina, P. *J. Org. Chem.* **2011**, *76*, 939–947. (g) Kwon, J. E.; Lee, S.; You, Y.; Baek, K. H.; Ohkubo, K.; Cho, J.;

- Fukuzumi, S.; Shin, I.; Park, S. Y.; Nam, W. *Inorg. Chem.* **2012**, *51*, 8760.
- (h) Kim, H. N.; Ren, W. X.; Kim, J. S.; Yoon, J. *Chem. Soc. Rev.* **2012**, *41*, 3210–3244. (i) Mandal, S.; Sikdar, Y.; Maiti, D. K.; Maiti, G. P.; Mandal, S. K.; Biswas, J. K.; Goswami, S. *RSC Adv.* **2015**, *5*, 72659. (j) Liu, B.; Tian, H. *Chem. Commun.* **2005**, 3156–3158. (k) Helal, A.; Lee, S. H.; Kim, S. H.; Kim, H. S. *Tetrahedron Lett.* **2010**, *51*, 3531.
- (2) (a) Hau, F. K. W.; He, X.; Lam, W. H.; Yam, V. W. W. *Chem. Commun.* **2011**, 47, 8778. (b) Chemate, S.; Sekar, N. *RSC Adv.* **2015**, *5*, 27282. (c) Kursunlu, A. N. *RSC Adv.* **2015**, *5*, 41025. (d) Xu, W.; Huang, D.; Su, M.; Wang, K.; Hong, M.; Zhou, Y. *Inorg. Chem.* **2014**, *53*, 6497. (e) Sun, X.; Wang, Y. W.; Peng, Y. *Org. Lett.* **2012**, *14*, 3420. (f) Lu, Y.; Huang, S.; Liu, Y.; He, S.; Zhao, L.; Zeng, X. *Org. Lett.* **2011**, *13*, 5274. (g) Chatterjee, N.; Maity, S. B.; Samadder, A.; Mukherjee, P.; Khudabukhsh, A. R.; Bharadwaj, P. K. *RSC Adv.* **2016**, *6*, 17995. (h) Pal, S.; Sen, B.; Mukherjee, M.; Patra, M.; Lahiri (Ganguly), S.; Chattopadhyay, P. *RSC Adv.* **2015**, *5*, 72508. (i) Qin, J. C.; Cheng, X.; Fang, R.; Wang, M.; Yang, Z.; Li, T.; Li, Y. *Spectrochim. Acta, Part A* **2016**, *152*, 352.
- (3) (a) Gu, B.; Huang, L.; Mi, N.; Yin, P.; Zhang, Y.; Tu, X.; Luo, X.; Luo, S.; Yao, S. *Analyst* **2015**, *140*, 2778. (b) Liu, X.; Gao, L.; Yang, L.; Zou, L.; Chen, W.; Song, X. *RSC Adv.* **2015**, *5*, 18177. (c) Xu, Y.; Pang, Y. *Chem. Commun.* **2010**, 46, 4070. (d) Liu, B.; Wang, J.; Zhang, G.; Bai, R.; Pang, Y. *ACS Appl. Mater. Interfaces* **2014**, *6*, 4402. (e) Zhang, Y.; Wang, J. H.; Zheng, W.; Chen, T.; Tong, Q. X.; Li, D. J. *Mater. Chem. B* **2014**, *2*, 4159. (f) Xu, Y.; Pang, Y. *Dalton Trans.* **2011**, 40, 1503. (g) Yang, C. C.; Tian, Y.; Chen, C. Y.; Jen, A.; Chen, W. C. *Macromol. Rapid Commun.* **2007**, *28*, 894. (h) Goswami, S.; Das, S.; Aich, K.; Pakhira, B.; Panja, S.; Mukherjee, S.; Sarkar, S. *Org. Lett.* **2013**, *15*, 5412. (i) Murale, D. P.; Kim, H.; Choi, W. S.; Churchill, D. G. *Org. Lett.* **2013**, *15*, 3946. (j) Ma, Q. J.; Zhang, X. B.; Zhao, X. H.; Gong, Y. J.; Tang, J.; Shen, G. L.; Yu, R. Q. *Spectrochim. Acta, Part A* **2009**, *73*, 687. (k) Maity, D.; Kumar, V.; Govindaraju, T. *Org. Lett.* **2012**, *14*, 6008. (l) Shyamal, M.; Mazumdar, P.; Maity, S.; Sahoo, G. P.; Salgado-Moran, G.; Misra, A. *J. Phys. Chem. A* **2016**, *120*, 210.
- (4) (a) Velmurugan, K.; Mathankumar, S.; Santoshkumar, S.; Amudha, S.; Nandhakumar, R. *Spectrochim. Acta, Part A* **2015**, *139*, 119. (b) Samanta, S.; Goswami, S.; Hoque, M. N.; Ramesh, A.; Das, G. *Chem. Commun.* **2014**, 50, 11833. (c) Reyes, J. F. G.; Barrales, P. O.; Diaz, A. M. *Talanta* **2005**, *65*, 1203. (d) Qin, J. C.; Yang, Z. Y. *Synth. Met.* **2015**, *209*, 570.
- (5) (a) Maity, D.; Govindaraju, T. *Inorg. Chem.* **2010**, *49*, 7229. (b) Huang, C. Y.; Jhong, Y.; Chir, J. L.; Wu, A. T. *J. Fluoresc.* **2014**, *24*, 991. (c) Wang, W.; Mao, Z.; Wang, M.; Liu, L. J.; Kwong, D. W. J.; Leung, C. H.; Ma, D. L. *Chem. Commun.* **2016**, 52, 3611. (d) Ma, J.; Shi, W.; Feng, L.; Chen, Y.; Fan, K.; Hao, Y.; Hui, Y.; Xie, Z. *RSC Adv.* **2016**, *6*, 28034. (e) Ali, R.; Razi, S. S.; Srivastava, P.; Shahid, M.; Misra, A. *RSC Adv.* **2015**, *5*, 61513. (f) Kar, C.; Samanta, S.; Goswami, S.; Ramesh, A.; Das, G. *Dalton Trans.* **2015**, 44, 4123. (g) Upadhyay, K. K.; Kumar, A. *Org. Biomol. Chem.* **2010**, *8*, 4892. (h) Sahana, A.; Banerjee, A.; Das, S.; Lohar, S.; Karak, D.; Sarkar, B.; Kanti Mukhopadhyay, S.; Mukherjee, A. K.; Das, D. *Org. Biomol. Chem.* **2011**, *9*, 5523. (i) Das, S.; Karak, D.; Lohar, S.; Banerjee, A.; Sahana, A.; Das, D. *Anal. Methods* **2012**, *4*, 3620. (j) Maity, D.; Govindaraju, T. *Eur. J. Inorg. Chem.* **2011**, 2011, 5479. (k) Park, H. M.; Oh, B. N.; Kim, J. H.; Qiong, W.; Hwang, I. H.; Jung, K. D.; Kim, C.; Kim, J. *Tetrahedron Lett.* **2011**, *52*, 5581. (l) Ding, W. H.; Cao, W.; Zheng, X. J.; Fang, D. C.; Wong, W. T.; Jin, L. P. *Inorg. Chem.* **2013**, *52*, 7320. (m) Kim, S.; Noh, J. Y.; Kim, K. Y.; Kim, J. H.; Kang, H. K.; Nam, S. W.; Kim, S. H.; Park, S.; Kim, C.; Kim, J. *Inorg. Chem.* **2012**, *51*, 3597. (n) Maity, D.; Govindaraju, T. *Chem. Commun.* **2010**, 46, 4499. (o) Maity, D.; Govindaraju, T. *Chem. Commun.* **2012**, 48, 1039.
- (6) (a) Jiang, J. H.; Wang, B. D.; Yang, Z. Y.; Liu, Y. C.; Li, T. R.; Liu, Z. C. *Inorg. Chem. Commun.* **2011**, 14, 1224. (b) Qin, J. C.; Yang, Z. Y.; Yang, P. *Inorg. Chim. Acta* **2015**, 432, 136. (c) Li, C. R.; Liao, Z. C.; Qin, J. C.; Wang, B. D.; Yang, Z. Y. *J. Lumin.* **2015**, *168*, 330. (d) Islam, A. S. M.; Bhowmick, R.; Mohammad, H.; Katarkar, A.; Chaudhuri, K.; Ali, M. *New J. Chem.* **2016**, *40*, 4710. (e) Hwang, I. H.; Choi, Y. W.; Kim, K. B.; Park, G. J.; Lee, J. J.; Nguyen, L. T.; Noh, I.; Kim, C. *New J. Chem.* **2016**, *40*, 171. (f) Guo, A.; Zhu, R.; Ren, Y.; Dong, J.; Feng, L. *Spectrochim. Acta, Part A* **2016**, *153*, 530. (g) Mukherjee, S.; Mal, P.; Stoeckli-Evans, H. *J. Lumin.* **2016**, *172*, 124.
- (7) Mameli, M.; Aragoni, M. C.; Arca, M.; Caltagirone, C.; Demartin, F.; Farruggia, G.; de Filippo, G.; Devillanova, F. A.; Garau, A.; Isaia, F.; et al. *Chem. - Eur. J.* **2010**, *16*, 919.
- (8) (a) Sauer, M. *Angew. Chem., Int. Ed.* **2003**, *42*, 1790. (b) Lu, Y.; Huang, S.; Liu, Y.; He, S.; Zhao, L.; Zeng, X. *Org. Lett.* **2011**, *13*, 5274. (9) Liu, Y.; Trogler, W. C. *Chem. Commun.* **2015**, 51, 14775. (10) Wu, J.; Liu, W.; Ge, J.; Zhang, H.; Wang, P. *Chem. Soc. Rev.* **2011**, *40*, 3483.
- (11) (a) Boonkitpatarakul, K.; Wang, J.; Niamnont, N.; Liu, B.; McDonald, L.; Pang, Y.; Sukwattanasinitt, M. *ACS Sens.* **2016**, *1*, 144. (b) Wang, J.; Pang, Y. *RSC Adv.* **2014**, *4*, 5845. (c) Adams, M. J.; Highfield, J. G.; Kirkbright, G. F. *Anal. Chem.* **1977**, *49*, 1850.
- (12) (a) Kemp, W. *Organic Spectroscopy*, 3rd ed.; Palgrave Macmillan, 1991. (b) Lakowicz, J. R. *Principles of Fluorescence Spectroscopy*, 3rd ed.; Springer, 2006. (c) Becke, A. D. *J. Chem. Phys.* **1993**, *98*, 5648. (d) Frisch, M. J.; Trucks, G. W.; Schlegel, H. B.; Scuseria, G. E.; Robb, M. A.; Cheeseman, J. R.; Scalmani, G.; Barone, V.; Mennucci, B.; Petersson, G. A.; Nakatsuji, H.; Caricato, M.; Li, X.; Hratchian, H. P.; Izmaylov, A. F.; Bloino, J.; Zheng, G.; Sonnenberg, J. L.; Hada, M.; Ehara, M.; Toyota, K.; Fukuda, R.; Hasegawa, J.; Ishida, M.; Nakajima, T.; Honda, Y.; Kitao, O.; Nakai, H.; Vreven, T.; Montgomery, J. A., Jr.; Peralta, J. E.; Ogliaro, F.; Bearpark, M.; Heyd, J. J.; Brothers, E.; Kudin, K. N.; Staroverov, V. N.; Keith, T.; Kobayashi, R.; Normand, J.; Raghavachari, K.; Rendell, A.; Burant, J. C.; Iyengar, S. S.; Tomasi, J.; Cossi, M.; Rega, N.; Millam, J. M.; Klene, M.; Knox, J. E.; Cross, J. B.; Bakken, V.; Adamo, C.; Jaramillo, J.; Gomperts, R.; Stratmann, R. E.; Yazyev, O.; Austin, A. J.; Cammi, R.; Pomelli, C.; Ochterski, J. W.; Martin, R. L.; Morokuma, K.; Zakrzewski, V. G.; Voth, G. A.; Salvador, P.; Dannenberg, J. J.; Dapprich, S.; Daniels, A. D.; Farkas, O.; Foresman, J. B.; Ortiz, J. V.; Cioslowski, J.; Fox, D. J. *Gaussian 09*, Revision C.01; Gaussian, Inc: Wallingford, CT, 2010. (e) Becke, A. D. *Phys. Rev. A: At., Mol., Opt. Phys.* **1988**, *38*, 3098. (f) Lee, C.; Yang, W.; Parr, R. G. *Phys. Rev. B: Condens. Matter Mater. Phys.* **1988**, *37*, 785. (g) Scalmani, G.; Frisch, M. J.; Mennucci, B.; Tomasi, J.; Cammi, R.; Barone, V. *J. Chem. Phys.* **2006**, *124*, 094107. (h) Cossi, M.; Rega, N.; Scalmani, G.; Barone, V. *J. Comput. Chem.* **2003**, *24*, 669.
- (13) (a) *SAINT and XPREP*, 5.1 ed.; Sheldrick, G. M., Ed.; Siemens Industrial Automation Inc: Madison, WI, 1995. (b) *SADABS, Empirical Absorption Correction Program*; University of Göttingen: Germany, 1997.
- (14) Sheldrick, G. M. *SHELXTL Reference Manual*, Version 5.1; Bruker AXS: Madison, WI, 1997.
- (15) Sheldrick, G. M. *SHELXL-97*, Program for Crystal Structure Refinement; University of Göttingen: Germany, 1997.
- (16) Spek, A. L. *PLATON-97*; University of Utrecht: The Netherlands, 1997.
- (17) *Mercury 3.1* (supplied with Cambridge Structural Database); CCDC, Cambridge, U.K., 2004.